X-ray and Nuclear Magnetic Resonance (NMR) Studies of Signalizing the Tripeptide Sequence (Tyr-D-Ala-Phe) of Dermorphin and Deltorphins I and II. Comparative Analysis in the Liquid and Solid Phases

Mikołaj M. Słabicki,[†,‡] Marek J. Potrzebowski,*[,†] Grzegorz Bujacz,[‡] Sebastian Olejniczak,[†] and Jacek Olczak[§]

Center of Molecular and Macromolecular Studies, Polish Academy of Sciences, Sienkiewicza 112, 90-363 Łódź, Poland, Institute of Technical Biochemistry, Technical University of Łódź, Stefanowskiego 4/10, 90-924 Łódź, Poland, and "TriMen" Ltd. Company, ul. Piłsudskiego 141, 92-318 Łódź, Poland

Received: October 29, 2003; In Final Form: February 5, 2004

The crystal and molecular structure of compound **1**, the "message" Tyr-D-Ala-Phe sequence of dermorphin and deltorphins I, II opioid peptides, was established using X-ray diffraction methods at a temperature of 100 K. Crystals of **1** are monoclinic, with the space group *C*2. The peptide chain has β-conformation. All three side groups are located on the same side of the peptide chain, because of the D-conformation of the central alanine (Ala). The H atoms of the methyl group create a C−H$\cdots\pi$ interaction with the phenyl ring of tyrosine (Tyr). The distances between the methyl group of D-Ala and the carbons of the phenyl ring of Tyr are in the range of 4.007−4.089 Å. NMR spectroscopy measurements were performed in the liquid and solid states, to conclude a higher-order structure of **1** in both phases and correlate with X-ray data. The PASS-2D experiment was used to assign principal elements of the chemical shift tensor ^{13}C δ_{ii}. The differences between the experimental values of ^{13}C δ_{ii} and the theoretical shielding parameters of ^{13}C σ_{ii} that are obtained using DFT GIAO calculation are explained in terms of distinction of the local motion of phenyl rings of Tyr and phenylalanine (Phe) at ambient temperature. ^{13}C T_1 measurements, analysis of the cross-polarization (CP) kinetics, and data obtained from dipolar dephasing experiment clearly proved the unique, dynamic features of tripeptide **1**.

1. Introduction

Recently, much attention has been given to the physiological properties and structural studies of opioid peptides, which are a promising and prospective group of painkiller drugs.[1] From a medical standpoint, these peptides act as morphine-like medicine and interact with the same group of receptors. There are three types of "classical" opioid receptors: δ, μ, and κ.[2] Knowledge of the structure and the preferred conformation of the substance acting with them is crucial to finding and designing new drugs. Recent progress in the X-ray diffraction (XRD) studies of opioid peptides was reviewed by Deschamps et al.[3] Hruby and Agnes exhaustively discussed the conformation−activity relationship of opioid peptides with selective activities at opioid receptors.[4] The substances that specifically bind to those receptors can be used for their mapping, to obtain the activity spectrum.

Dermorphin and deltorphins are natural opioid peptides that have been isolated from frogs (*Phyllomedusa bicolor, Phyllomedusa sauvagei)* that live on the border of Brazil and Peru and secrete a mixture of peptides through their skin.[5] Dermorphin (Tyr-D-Ala-Phe-Gly-Tyr-Pro-Ser-NH2) is the first known peptide produced by a eukaryote that contains D-amino acid,[6] because post-translation modification of this peptide includes conversion of L-alanine to its D-isomer. Dermorphin binds to the μ-selective opioid receptor[7] and induces, for example, long-lasting analgesia, especially on the central nervous system, and is up to a 1000-fold greater than that from morphine.[8] The "message" domain, which is responsible for this interaction, is a tripeptide, Tyr-D-Ala-Phe (**1**). This short sequence is also present in deltorphins I (Tyr-D-Ala-Phe-Asp-Val-Val-Gly-NH2) and deltorphins II (Tyr-D-Ala-Phe-Glu-Val-Val-Gly-NH2) in the secretion products of *P. sauvagei.* In the message sequence of deltorphin, D-Ala is replaced by D-Met (deltorphin Tyr-D-Met-Phe-His-Leu-Met-Asp-NH2).[9] ^{1}H NMR studies that were performed in two different solvents showed that the conformational preferences of the N-terminal sequence of the peptide are similar.[10] Deltorphins have the highest selectivity toward δ-receptors of all the natural opioid peptides. The C-part of the dermorphin and the deltorphins is an "address" sequence, which causes the selectivity of those peptides. On the basis of the structural studies, it is believed that the critical factor that determines the activity of opioid peptides is the relative orientation between the Tyr and Phe in the tripeptide sequence.[11] μ- and δ-receptors recognize the β-turn in the N-terminal part of dermorphin and deltorphins. In the liquid phase, their affinity and activity was discussed in terms of changes of conformation of the side chain tyrosine (Tyr) and phenylalanine (Phe).[12]

Despite many attempts to precisely assign the topology of the message Tyr-D-Ala-Phe sequence, this question is still the challenge for structural chemistry. Many authors have studied the conformational analysis of dermorphin, deltorphins, and their shorter peptide analogues, using, for this purpose, mostly NMR spectroscopy in a liquid phase and a molecular modeling approach.[13] In this paper, we report the X-ray crystal data and molecular structure of Tyr-D-Ala-Phe **(1)**. Our structural X-ray studies are supported by NMR measurements in the solid phase.

* Author to whom correspondence should be addressed. E-mail address: marekpot@bilbo.cbmm.lodz.pl.
[†] Polish Academy of Sciences.
[‡] Technical University of Łódź.
[§] "TriMen", Ltd.

10.1021/jp0372690 CCC: $27.50
Published on Web 03/12/2004

Comparative analysis of the structure in the liquid and solid states is accomplished by inspection of the NMR data measured in both phases.

2. Experimental Section

2.1. X-ray Diffraction. Five milligrams of lyophilized rough product was dissolved in 1 mL of methanol and 0.2 mL of H_2O and then crystallized via a vapor diffusion method, using ethyl acetate as the precipitating solvent. The crystals had a triangular platelike morphology and grew in the form of clusters. The species, which had dimensions of 80 μm × 150 μm × 10 μm, was separated from the clusters and affixed with glue on top of a glass capillary. The data were collected on the X-13 beam line (EMBL, Hamburg, Germany), using a MAR CCD 165-mm detector. Two runs, corresponding to high and low resolution, were performed. The X-ray dosage for the low-resolution run was 10 times lower than that for the high-resolution run, to avoid overload reflections. The data were processed using DENZO and scaled using SCALEPACK. Experimental details from data collection and data processing are listed in Table 1. All observed reflections with $I > 0\sigma(I)$ were used to solve the structure by direct methods and to refine it by full matrix least-squares using F's.[14,15] H atoms were observed on the difference Fourier map and refined isotropically. Anisotropic thermal parameters were refined for all non-H atoms. The structure was solved by the DIRECT method, using SHELXS,[14] and was refined using SHELXL.[15] The need for good statistical parameters for data processing and structure refining dictated the use of synchrotron radiation for structural analysis of very small crystals. Crystal data were deposited in the Cambridge Crystallographic Data Centre (Deposit No. CCDC 222456).[46]

2.2. NMR Measurements. NMR spectra in the liquid phase were recorded on a spectrometer (Bruker, model Avance DRX 500) that was operating at 500.13 MHz for ^{1}H and 125.26 MHz for ^{13}C. The spectrometer was equipped with a pulse field gradient (PFG) unit (50 G/cm). Five milligrams of sample was dissolved in 0.5 mL of the methanol-d4. With such a concentration, the ^{13}C and 2D NMR spectra were measured. ^{1}H spectra were recorded at concentrations that were 5-fold lower. The chemical shift of the methanol signal (methyl group) was used as a reference (δ_H 3.31; δ_C 48.50).

The solid-state cross-polarization magic angle spinning (CP MAS) ^{13}C NMR experiments were performed on a spectrometer (Bruker, model Avance DSX 300), at a frequency of 75.47 MHz, that was equipped with a MAS probe head, using 4-mm ZrO_2 rotors. A sample of glycine (Gly) was used to set the Hartmann−Hahn condition and adamantane was used as a secondary chemical-shift reference (δ = 38.48 and 29.46 ppm from external tetramethylsilane (TMS)).[16] The conventional spectra were recorded with a proton 90° pulse length of 3.5 μs and a contact time of 1 ms. The repetition delay was 10 s, and the spectral width was 25 kHz. Free induction decay (FID) spectra were accumulated with a time domain size of 2K data points. The RAMP shape pulse was used during the cross polarization and two-pulse phase modulation (TPPM), with $\tau_p = 6.8$ μs and a phase angle of 20° during the acqusition. The cross-polarization efficiency was measured with contact times between 10 μs and 12 ms. The spectra data were processed using the WIN NMR program.[17]

A sample spinning speed of 2 kHz (600 Hz for the aliphatic region) was used in PASS-2D experiments.[18] The 16-point t_1 experiment data were replicated to 256 points. One-dimensional CSA spinning sidebands was obtained from t_1 slices that were taken at isotropic chemical shifts in the ω_2 dimension of the 2D spectrum. The magnitudes of the principal elements of the chemical shift anisotropy (CSA) were obtained from the best-fitting simulated spinning patterns. Simulations of the spinning CSA sidebands spectra were performed on a personal computer (PC), using the SIMPSON program under the LINUX environment.[19]

DFT GIAO calculations were performed using a GAUSSIAN 98 program that was running on a Silicon Graphics Power Challenge computer.[20] The GIAO method, with the B3PW91 hybrid method and 6-311++G** basis set, was used to calculate the NMR parameters.

^{13}C T_1 relaxation times of **1** in a methanol−water solution (1/1 v/v) were measured by means of a SUFIR sequence.[21] In the solid state, ^{13}C T_1 parameters were measured at room temperature, by means of a Torchia sequence.[22]

TABLE 1: Crystal Data and Experimental Details of 1

parameter	value
Crystal Data	
molecular formula	$C_{21}H_{25}N_3O_5$
molecular weight	399.44
crystal system	monoclinic
space group	*C*2
lattice parameters	
a	23.091(5) Å
b	5.4940(10) Å
c	17.510(4) Å
β	117.88(3)°
volume, V	1963.5(7) Å^3
Z	4
density, D_c	1.351 g/cm^3
μ	0.97 cm^{-1}
Measurement Details	
wavelength	0.803 Å
maximum 2θ	64.72°
T_{meas}	100 K
high-resolution run	
number of images	90
$\Delta\phi$	4.0°
resolution	99.0−0.75 Å
low-resolution run	
number of images	45
$\Delta\phi$	8.0°
resolution	99.0−1.15 Å
Data Processing	
resolution	99.0−0.75 Å (0.78−0.75)
Rmerge	4.5% (9.5)
completeness	98.0% (97.0)
number of reflections	17426
number of unique reflections	2631
redundancy	6.62 (5.92)
I/sigma$\langle I \rangle$	31.02 (14.44)
Refinement Statistics	
number of reflections	
unique[a]	4769
with $I > 0\sigma(I)$	4739
observed with $I > 2\sigma(I)$	4627
number of parameters refined	363
largest diffraction peak	0.370 e/Å^3
largest diffraction hole	−0.206 e/Å^3
shift/esd max	0.001
R_{obs}	0.0394
wR_{obs}	0.1027
S_{obs}	1.041
weighting coefficient[b]	
m	0.0642
n	0.5904
extinction coefficient, k[c]	0.0189 (17)
F(000)	848

[a] Friedel pairs kept separately. [b] Weighting scheme: $w = [\sigma^2(Fo^2) + (mP)^2 + nP]^{-1}$, where $P = (Fo^2 + 2Fc^2)/3$. [c] Extinction method SHELXL, using the extinction expression $Fc^* = [1 + 0.001(Fc^2\lambda^3/\sin(2\theta))]^{-1/4}$.

SCHEME 1. Synthesis of Tripeptide 1

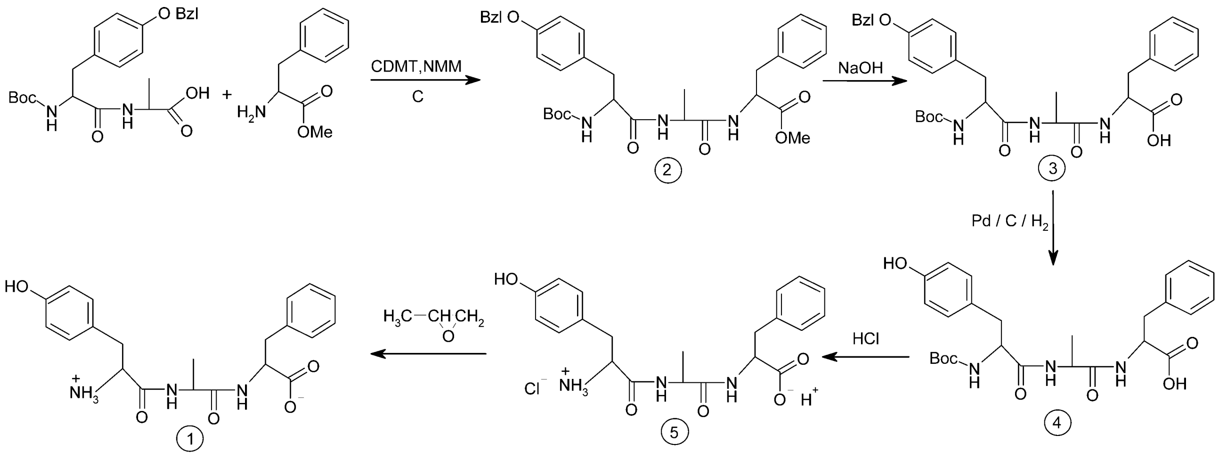

2.3. Synthesis of Peptide. 2.3.1. Synthesis of Boc-Tyr(Bzl)-D-Ala-PheOMe (**2**, $C_{34}H_{41}N_3O_7$; MW = 603.72). 4-Methylmorpholine (NMM) (0.134 g, 1.33 mmol) was added to the solution of chlorodimethoksytriazine (CDMT) (0.233 g, 1.33 mmol) in dry dichloromethane (5.3 mL), and the resulting slurry was stirred at a temperature of 0 °C for 30 min. The dipeptide Boc-Tyr(Bzl)-D-Ala-OH (0.586 g, 1.33mol) then was added and the mixture was stirred at 0 °C for an additional 30 min. Then, 0.300 g (1.40 mol) of HCl.H-L-Phe-OMe and a second portion of NMM (0.134 g, 1.33 mmol) were added. The cooling bath was removed, and the resulting mixture was stirred at room temperature overnight. The reaction mixture was diluted with ethyl acetate (50 mL), then washed with water, 2M HCl, 1M K_2CO_3, and brine, and finally dried over $MgSO_4$. The solution then was filtered, and the solvent was evaporated. The crude product was purified in a column that was packed with silica gel (elution with a 1/1 ethyl acetate/hexanes mixture) to give 0.425 g (0.70 mmol, 52.9%) of pure product.

2.3.2. Synthesis of Boc-Tyr(Bzl)-D-Ala-Phe-OH (**3**, $C_{33}H_{39}N_3O_7$; MW = 589.69). Compound **2** was dissolved in methanol (5 mL) and 1N NaOH (3 mL) was added. The reaction mixture was stirred at room temperature until the starting material was undetectable by thin-layer chromatography (TLC) (ca. 3 h). The mixture then was partitioned between ethyl acetate (30 mL) and 0.5N HCl (20 mL). An aqueous layer was extracted with ethyl acetate (20 mL) once more, and the organic solutions were collected and dried over $MgSO_4$. The evaporation of solvent gave 0.201 g (0.34 mmol, 48.4%) of the chromatographically homogeneous product (via TLC, with a 20/1 $CHCl_3$/MeOH mixture).

2.3.3. Synthesis of Boc-Tyr-D-Ala-Phe-OH (**4**, $C_{26}H_{33}N_3O_7$; MW = 499.57). Compound **3** was placed in a three-neck round-bottomed flask and dissolved in 20 mL of methanol. The flask was flushed with argon and 10 mg of palladized (10%) charcoal was added with care. The argon-filled balloon was replaced by a hydrogen-filled one. The flask was flushed with hydrogen, and the reaction mixture was stirred under hydrogen until the starting material could no longer be detected by TLC (using a 20/1 $CHCl_3$/MeOH mixture). The solution was filtered through a pad of Celite, and the celit was washed several times with small portions of methanol. The filtrates were collected and evaporated to dryness. The resulting solid was triturated with 20 mL of a 1/1 diethyl ether/hexanes mixture, filtered, and then dried overnight in a desiccator over P_2O_5 (0.120 g, 0.24 mmol, 70.6%). It was sufficiently pure (via high-performance liquid chromatography (HPLC) and TLC) to be used in the next step without further purification.

2.3.4. Synthesis of HCl.H-Tyr-D-Ala-Phe-OH (**5**, $C_{21}H_{25}N_3O_5$ (+ HCl); MW = 399.45 (+ 36.46)). Compound **4** was placed in the round-bottomed flask, protected from moisture; 2 mL of 4N HCl in dioxane was added, and the reaction mixture was stirred for 1 h at room temperature. The solvent was removed under reduced pressure (bath temperature of 35 °C). Diethyl ether was added to the resulting solid, and the solid was triturated. The product was allowed to settle and the ether layer was removed with a Pasteur pipet. A new portion of ether was added and the operation was repeated once more. After the ether had been removed, the product was placed in a desiccator over KOH and P_2O_5 and dried under vacuum overnight. The yield was 0.081 g (0.186 mmol, 77.4%).

2.3.5. Synthesis of H-Tyr-D-Ala-Phe-OH (**1**, $C_{21}H_{25}N_3O_5$; MW = 399.45). The peptide hydrochloride **5** was dissolved in 2 mL of methanol and 200 μL of propylene oxide was added. The resulting mixture was gently heated in a tightly stoppered flask for 3 h. After the mixture was cooled to the ambient temperature, the precipitate of a zwitterionic peptide was filtered and washed with a small portion of methanol and several portions of diethyl ether. The product was placed in a desiccator over KOH and P_2O_5 and dried under vacuum overnight. The yield was 0.062 g (0.155 mmol, 83.3%).

3. Results

3.1. Synthesis. The solid-phase synthesis of tripeptide **1** was reported elsewhere.[23] In this work, we report a method that describes a "wet" procedure. Synthesis of **1** was performed by TriMen Chemicals, Ltd. Scheme 1 presents the synthesis pathway in pictorial form. The blocked dipeptide Tyr-D-Ala was used as the starting substrate. Details concerning each step of synthesis, blocking, and deblocking of the peptides are given in the Experimental Section.

3.2. X-ray Data. The crystals of Tyr-D-Ala-Phe **1** are monoclinic, with space group *C*2. Crystal data and experimental details are collected in Table 1. The molecular structure and numbering system is shown in Figure 1.

The unit cell consists of four molecules, with one molecule in an asymmetric unit. The peptide molecule exists in zwitterionic form, with a positively charged terminal amine group and a deprotonated carboxylic group. The distances between C30 and the appropriate O atoms are 1.248(2) Å for C30−O30 and 1.262(2) Å for C30−O31. These values suggest that a higher fraction of negative charge is located on the O31 atom. The geometrical parameters, bond lengths, and bond and torsion angles are obtained from the CCDC data (Deposit No. CCDC 222456).

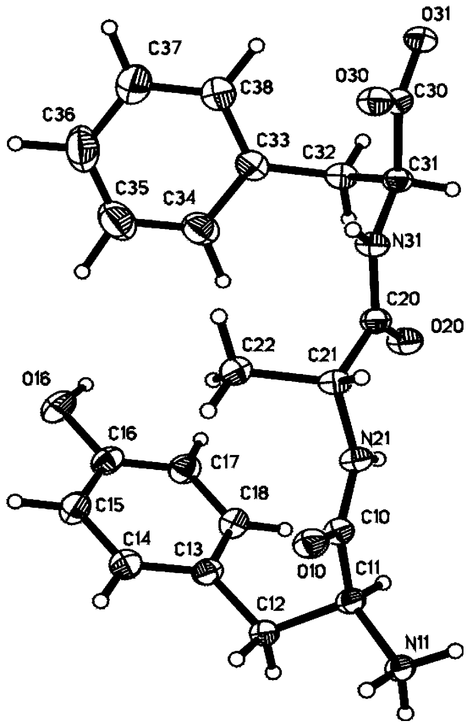

Figure 1. Molecular structure of tripeptide **1** with labels of non-H atoms, with ellipsoids at 50% probability.

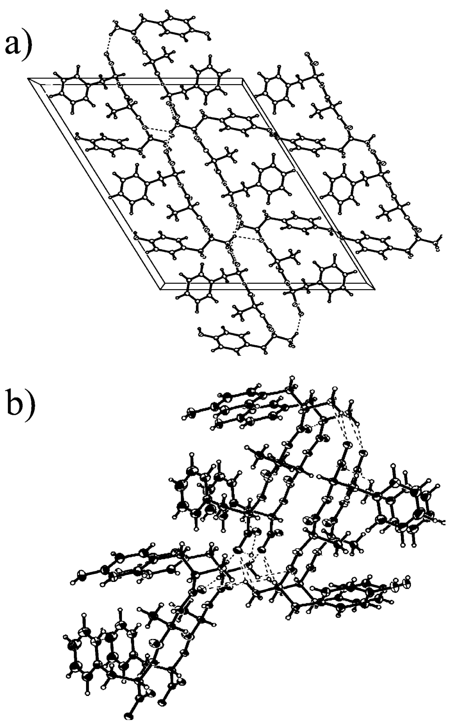

Figure 2. (a) Unit cell containing four molecules of tripeptide **1** and (b) a depiction of six molecules of tripeptide **1**. Both pictures reflect their interactions between molecules with ellipsoids at 50% probability.

The molecular packing of the unit cell is depicted in Figure 2. The peptide chain has β-conformation. There are weak interactions in the *b*-direction, which are responsible for the creation of a pseudo-parallel β-sheet in the *x,y* plane. All three side groups are located on the same side of the peptide chain, because of the D-conformation of the central Ala. Two aromatic π-rings of Tyr and Phe are slanting toward each other, at an angle of 60.03(4)°. The distances between the methyl group of D-Ala and the C atoms of the phenyl ring of Tyr are in the range of 4.007−4.089 Å. The H221 atom creates a weak hydrogen interaction with the phenyl ring of Tyr.

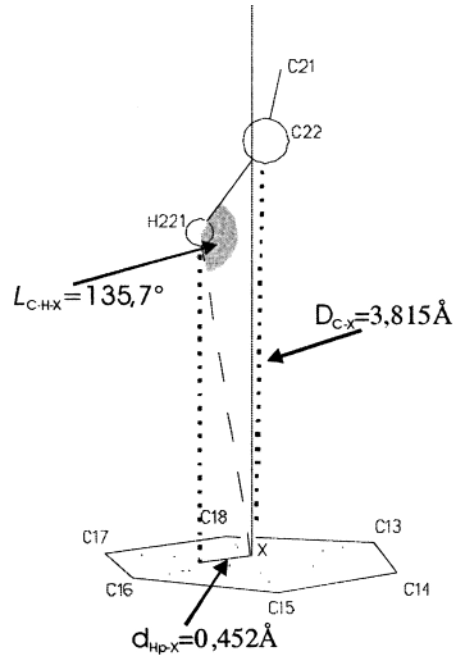

Figure 3. C22− H221 interaction with a π-electron system of tyrosine. Notation and definitions of d_{C-X}, $\angle_{C-H-X}$, and d_{Hp-X} also are given in the figure.

The criteria suggested by Brandl et al.[24] for $C_{ali}-H\cdots\pi$ interactions are as follows: $d_{C-X} \leq 4.5$ Å (the distance between the C atom and the center of the π-system), $\angle_{C-H-X} \leq 120°$ (the angle at the H atom of the donor group), and $d_{Hp-X} \leq 1.2$ Å (the distance of the H-atom position projected vertically onto the π-plane from atom X). The C22−H221 bond, with the Tyr ring, creates an interaction of the following parameters: $d_{C-X} = 3.815$ Å, $\angle_{C-H-X} = 135.7°$, and $d_{Hp-X} = 0.452$ Å (see Figure 3). Inspection of Figure 3 shows that $C-H\cdots\pi$ contact is possible, because of the D-conformation of the central Ala. There is no such interaction of the D-Ala side chain and Phe. Even when the data collections were performed at a temperature of 100 K, the thermal vibration of the aromatic ring of Phe is greater than that of the ring of Tyr. The average isotropic thermal factors for Phe and Tyr side chains are 0.0275 and 0.0419, respectively, so they differ by 52.4% in comparison to Phe, which may suggest higher flexibility of the phenylalanine side chain.

The two molecules of **1** form a head-to-tail type of dimer that is joined via hydrogen bonding (see Table 2). The hydrogen bonds that are responsible for dimer formation occur between the O31 atom from the carboxyl moiety and H11N (O31⋯H11N, 2.04(2) Å). The peptide chains are parallel with the hydrophobic side chains stacking outward, relative to each other. The crystallographic 2-fold axes pass through the center of the dimer. The α-carbon of the D-Ala is facing the α-carbon of the Phe from the opposite side of the dimer. In the crystal lattice, the carboxyl group forms additional hydrogen bonds with amino groups. The O31 atom creates a second intramolecular hydrogen bond with H13N (O31⋯H13N, 1.72(2) Å). The other oxygen atom from the carbonyl (O30) is involved in only one intramolecular hydrogen bond with H12N (O30⋯H12N, 1.78(2) Å) and one long intermolecular hydrogen bond with N31N (O30⋯H31N, 2.13(2) Å). Weaker hydrogen bonds for the O30 atom are responsible for the longer distance from carbon, in comparison to the O31 atom (which suggests that a lower

TABLE 2: Selected Hydrogen-Bonding Geometry for Tripeptide 1[a]

D−H···A	D−H (Å)	H···A (Å)	D···A (Å)	D−H···A (deg)
N11−H11N···O10i	0.92(2)	2.48(3)	3.019(2)	117.7(19)
N11−H11N···O31i	0.92(2)	2.04(2)	2.877(1)	152.1(22)
N11−H12N···O10i	0.96(2)	2.76(2)	3.019(2)	96.4(15)
N11−H12N···O30ii	0.96(2)	1.78(2)	2.726(2)	170.6(21)
N11−H13N···O31iii	0.98(2)	1.72(2)	2.692(2)	171.6(22)
O16−H16O···O16iv	0.94(4)	2.03(4)	2.924(2)	158.8(33)
N11−H13N···O10	0.98(2)	2.58(3)	2.833(2)	94.8(15)
N21−H21N···O20	0.92(2)	2.16(2)	2.593(2)	107.8(15)
N31−H31N···O30	0.84(3)	2.13(2)	2.578(2)	113.1(19)

[a] H···A ≤ 2.80 Å. Symmetry codes were as follows: (i) $1.5 - x, y - 0.5, 1 - z$; (ii) $0.5 + x, y - 0.5, z$; (iii) $0.5 + x, 0.5 + y, z$; and (iv) $1.5 - x, y - 0.5, 2 - z$.

negative charge exists on the O30 atom). In a hydrophobic layer, there is a relatively strong hydrogen bond between two neighboring Tyr molecules (O16···H16O, 2.03(4) Å), which are related by a 2-fold axis, which increases the length of the O16−H16O bond to 0.94(4) Å. The O10 atom interacts with H11N and creates a weak hydrogen bond, with a bond length of 2.48(3) Å; however, it simultaneously forms an intermolecular bond with H13N (bond length of 2.58(3) Å). Another intermolecular interaction, of medium strength, is observed in the form of the connection between the O30 atom and H31N (2.13(2) Å).

3.3. NMR Analysis. 3.3.1. NMR Studies of **1** in Solution and Solid State. The 1D and 2D ^{1}H and ^{13}C NMR spectra were analyzed (i) to obtain the complete assignment of proton and C chemical shifts and (ii) to elucidate the structure of tripeptide **1**. In some experiments in solution, we have taken advantage of the pulse field gradient (PFG) system to reduce the time of measurement and improve the quality of spectra. The ^{1}H and ^{13}C chemical shifts, as well as the proton−proton *J* coupling constants, were established by means of ^{1}H−^{1}H PFG COSY (correlation spectroscopy), ^{1}H−^{1}H PFG TOCSY (totally correlated spectroscopy), ^{1}H−^{13}C PFG HMQC (heteronuclear multiple quantum coherence), and ^{1}H−^{13}C PFG HMBC (heteronuclear multiple bonds coherence) experiments. The HMBC experiment was optimized for $^{3}J = 5$ Hz. The ^{1}H chemical shifts and the values of geminal (^{2}J) and vicinal (^{3}J) coupling constants for **1** are given in Table 3.

The ^{13}C CP/MAS spectrum of **1**, recorded at 7 kHz with RAMP shape CP[25] and TPPM decoupling,[26] is shown in Figure 4a. The preliminary assignment of the isotropic chemical shifts for **1** was done by data comparison with those obtained in the liquid phase (see Figure 4b). ^{13}C δ_{iso} data for both phases also are collected in Table 3. Comparative analysis of the chemical shift parameters clearly shows that the conformation of tripeptide in the liquid and solid states is basically similar. The biggest difference is seen for the carbonyl group of C20 ($\Delta = 4.2$ ppm), aliphatic carbons of methylene C32 ($\Delta = 4.2$ ppm), methine groups C31 ($\Delta = 3.1$ ppm), and aromatic C16 carbon ($\Delta = 3.6$ ppm).

However, it is well-known that more information about the electronic surroundings of each nucleus, which reflects subtle structural effects, can be obtained from inspection of the tensorial nature of the chemical shift. Hence, in this part of the project, we were attracted by the prospect of the analysis of ^{13}C δ_{ii} data for **1**, the inspection of anisotropic values of the chemical shift tensors (CSTs), and correlation of the principal elements to the molecular structure.

For rotating solids, ^{13}C δ_{ii} parameters can be obtained from the analysis of the intensities of the spinning sidebands. For the sample under investigation, the spinning rate should be in range of 2−3 kHz, to obtain a spectrum with a sufficient number of sidebands for further calculations of the aromatic and carboxyl/carbonyl region. For aliphatic signals, the spinning rate should be even smaller, in range of a few hundred Hz. As we observed in the case of **1**, the deconvolution procedure is not an easy task. At low spinning speeds (see Figure 4c), the overlap between different manifolds of the spinning sidebands and the analysis of the spectrum is ambiguous. Separation of the isotropic and anisotropic components of the spectra with heavy overlapped systems is still a challenge for solid-state NMR spectroscopy. Several approaches can be used to achieve this goal.[27] In our project, we used the PASS-2D sequence, which, compared to other techniques, offers good sensitivity and does not require any hardware modifications or a special probe head. A detailed explanation of the PASS-2D pulse sequence, its performance, a *Mathematica* routine to generate a set of PASS solutions, and the data processing can be found elsewhere.[18,28]

TABLE 3: Values of ^{1}H Chemical Shifts and Coupling Constants, and ^{13}C Isotope Chemical Shifts in the Liquid and Solid States

^{1}H Chemical Shifts

	chemical shift (ppm)
H22	0.87
H321	2.88
H121	2.98
H122	3.09
H322	3.21
H11	4.02
H21	4.17
H31	4.44
H15, H17	6.81
H14, H18	7.09
H34, H38	7.20
H36	7.21
H35, H37	7.27

^{1}H Coupling Constants

	coupling constant ^{2}J, ^{3}J (Hz)
H21−H22	7.00
H311−H321	8.50
H311−H322	4.50
H321−H322	13.50
H11−H121	8.75
H11−H122	6.50
H121−H122	13.50
H14,H18−H15,H17	8.25

^{13}C Chemical Shifts

	chemical shift (ppm) liquid state	chemical shift (ppm) solid state
C22	17.7	20.3
C32	39.0	34.8
C12	37.3	37.8
C21	50.1	48.2
C11	55.7	54.1
C31	57.2	54.1
C17	116.6	114.9
C15	116.6	115.5
C36	127.5	125.3
C35	129.2	126.4
C37	129.2	126.4
C13	126.4	128.2
C34	130.4	128.8
C38	130.4	128.8
C18	131.6	129.9
C14	131.6	132.1
C33	138.8	136.5
C16	156.8	153.2
C10	169.5	167.2
C20	173.4	169.2
C30	178.2	177.0

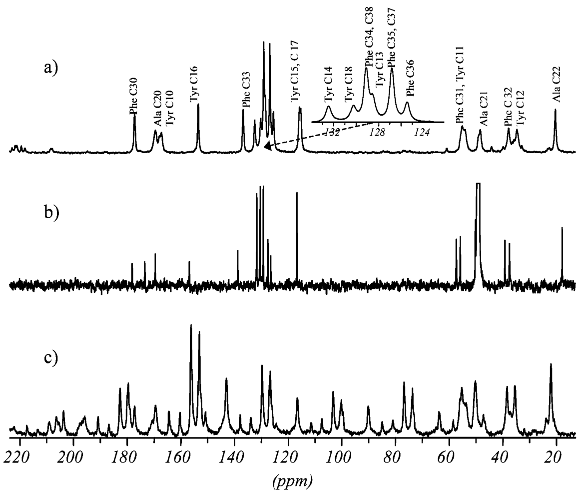

Figure 4. ^{13}C NMR spectra of tripeptide **1**: (a) CP/MAS at 7 kHz with RAMP shape cross-polarization and TPPM decoupling, (b) liquid phase (methanol), and (c) CP/MAS at 2 kHz.

Figure 5 displays the PASS-2D spectrum of **1**, which was recorded with a spinning rate of 2 kHz. The carbonyl group and aromatic atoms are characterized by large CSA and, under slow sample spinning, present a complex pattern. Through proper data shearing (see Figure 5b), it is possible to separate the spinning sidebands for each C atom and, using a calculation procedure, establish the ^{13}C δ_{ii} parameters. Such a presentation clearly shows that the F2 projection corresponds to a TOSS[29] spectrum, whereas F1 represents CSA.

In this work, ^{13}C δ_{ii} values were obtained by means of the SIMPSON program.[19] The ^{13}C shielding parameters are collected in Table 4. The experimental and the best-fitting simulated 1D spinning CSA sideband patterns for selected C atoms of **1** are shown in Figure 6.

The ^{13}C δ_{ii} values that have been completed in our project were compared with data reported by Ye at al.[30] for corresponding free amino acids. In principle, for carboxyl and aromatic signals, the CST values are roughly similar to the literature data, with exception of the data for the C34 and C38 carbons of phenylalanine. In the cited paper, these carbons are axially symmetric, with $\delta_{11} = 182 \pm 6$, $\delta_{22} = 182 \pm 6$, and $\delta_{33} = 23 \pm 5$. ^{13}C δ_{ii} elements for the carboxyl group (C30) are typical for the deprotonated, zwitterionic form of amino acids.[31,32] The CST values of peptide carbons (C10 and C20) require a short comment. Ando et al. reported a linear correlation

TABLE 4: Values of the Experimental Chemical Shift Parameters δ_{ii} and Corresponding Anisotropic Parameters[a]

^{13}C	δ_{11} (ppm)	δ_{22} (ppm)	δ_{33} (ppm)	Ω (ppm)	κ (ppm)
C22	41	14	6	35	−0.51
C32	47	38	19	28	0.38
C12	53	39	21	33	0.15
C21	69	47	29	41	−0.12
C11	69	55	38	31	0.10
C31	69	55	38	31	0.10
C17	191	130	24	167	0.27
C15	193	128	25	167	0.23
C36	222	118	36	187	−0.12
C35	174	157	48	127	0.73
C37	174	157	48	127	0.73
C13	221	146	18	203	0.27
C34	175	157	54	121	0.70
C38	175	157	54	121	0.70
C18	223	148	18	205	0.27
C14	224	142	31	192	0.15
C33	233	137	39	194	0.01
C16	239	153	67	172	−0.01
C10	244	164	94	150	−0.06
C20	246	172	90	156	0.06
C30	237	186	107	130	0.21

[a] Estimated error in δ_{11}, δ_{22}, and δ_{33} is ±3 ppm; span is expressed as $\Omega = \delta_{11} - \delta_{33}$, and skew is expressed as $\kappa = 3(\delta_{22} - \delta_{iso})/\Omega$.

between the ^{13}C δ_{ii} parameters and the strength of the >C═O···H−N< hydrogen bonding.[33]

The orientation of the ^{13}C principal elements of CST, with respect to the molecular frame of the amide carbonyl carbon, is shown in Scheme 2.

The δ_{11} component is in the amide sp^2 plane and lies along a direction normal to the C═O bond, whereas the δ_{22} component lies almost along the amide C═O bond and the δ_{33} component is aligned perpendicular to the amide sp^2 plane. It is apparent that the most-sensitive parameter, which best reflects the nature of hydrogen bonding, is δ_{22}. X-ray data (see Table 2) clearly suggest that both amide carbonyl carbons are involved, rather than in intramolecular contacts. The intermolecular hydrogen bond between the C(10)═O assembly and the amine protons is relatively weak ($R_{N\cdots O}$ = 3.0192 Å). The values of the δ_{22} components established for amide carbons (174 and 172 ppm for C(20)═O and C(10)═O, respectively) are typical for systems that are loosely bonded and are consistent with literature data.[33]

CST parameters of α- and β-carbons of amino acids, which are the building units of peptides, have recently received much attention, because knowledge of the ^{13}C δ_{ii} values also provides information about the higher-order structures of oligopeptides.[34] Figure 7 displays the PASS-2D spectrum of the aliphatic region,

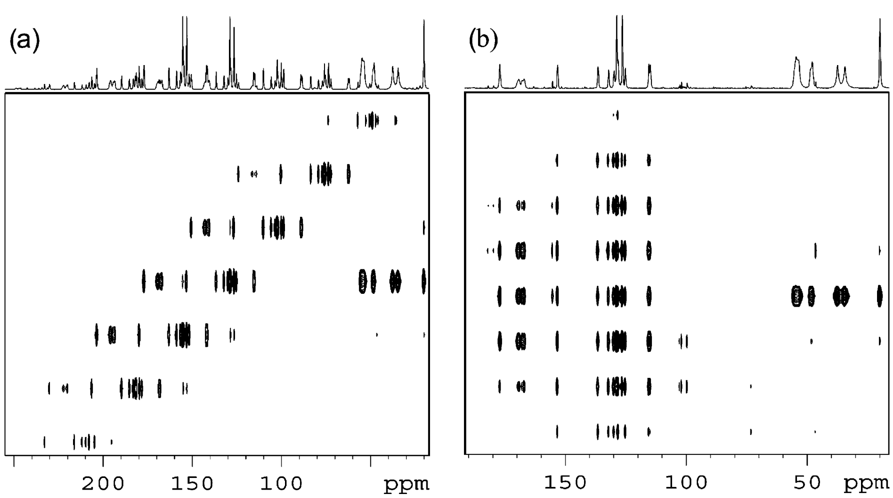

Figure 5. PASS-2D spectrum of tripeptide **1** (a) recorded with a spinning rate of 2 kHz and (b) after proper data shearing.

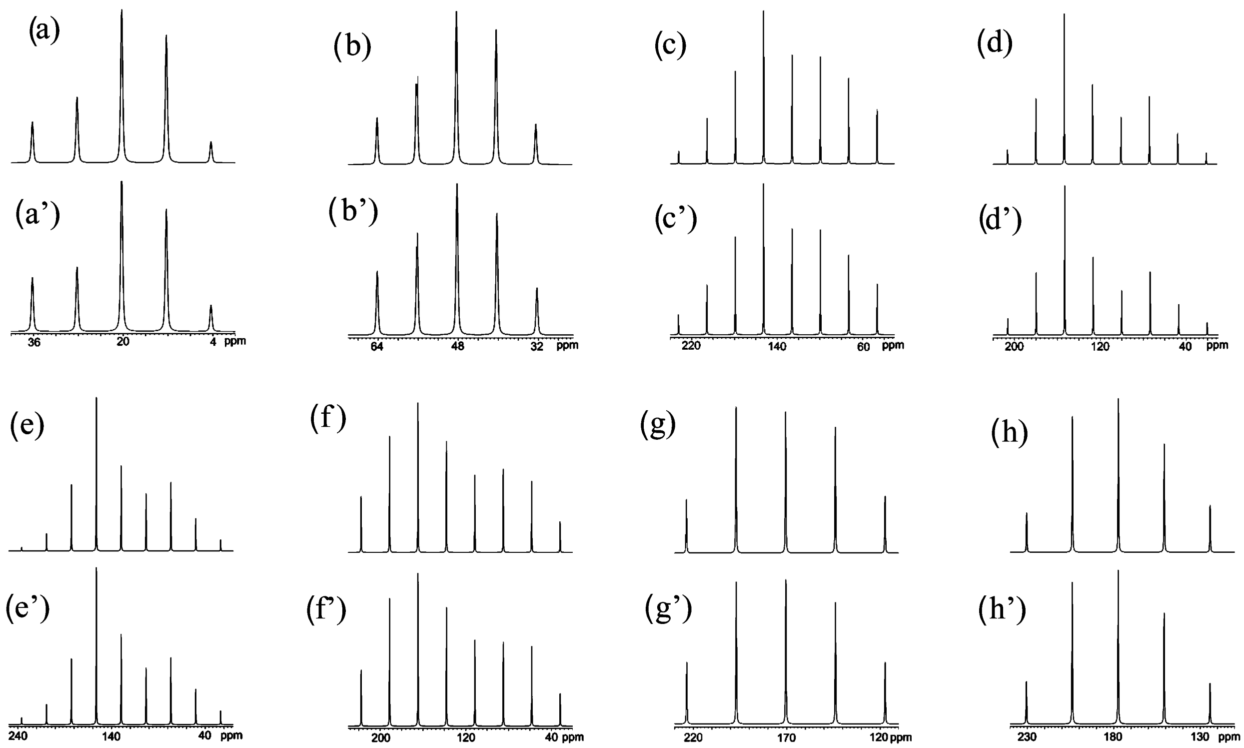

Figure 6. Experimental and best-fitting simulated 1D spinning CSA sideband patterns for (a) C22, (b) C21, (c) C36, (d) C35, C37, (e) C38, C34, (f) C33, (g) C20, and (h) C30. Regularly labeled panels represent experimental patterns, whereas labels with a prime symbol represent best-fit patterns.

SCHEME 2. Orientation of the ^{13}C Principal Elements of the Chemical Shift Tensor Components, with Respect to the Bond Geometry

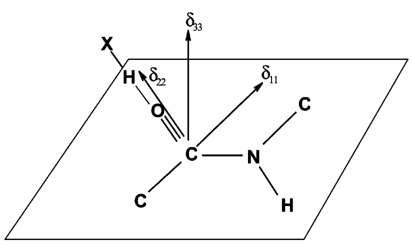

recorded with a spinning rate of 600 Hz. As in the case of the aromatic and carbonyl signals, a similar methodology was used to obtain data from the PASS-2D cross section. The best-fitted results are given in Table 4.

3.3.2. DFT GIAO Calculations. In this section, we used a theoretical approach to verify the correctness of the structural assignments. Several methods are currently available for the computation of NMR parameters.[35] In our work, the GIAO B3PW91 hybrid method was used for the calculation of the ^{13}C parameters of **1**. The XRD data of **1** was used as an input file. The advantage of such an approach is related to the fact that it is possible to compare the theoretical and experimental results for molecules with exactly the same geometry of heavy atoms. The position of the H atoms must be optimized, because locating protons accurately via XRD is often difficult. The theoretical ^{13}C chemical shift parameters that have been calculated by means of the GIAO method for **1** are collected in Table 5.

Figure 8a shows the correlation of the experimental isotropic chemical shift versus the isotropic theoretical shielding parameters. The obtained results clearly prove the correctness of the assignment of the isotropic values of the chemical shift. An interesting correlation was obtained when comparing ^{13}C δ_{ii} versus σ_{ii} components. In this case, the comparison of experimental data versus theoretical data was much worse (see Figure 8b). Several points do not follow the linear relationship, and it is intriguing to note that these points primarily represent the phenylalanine residue. The scatter effect is even more visible when the span parameters Ω are compared (Figure 9). It is apparent from this plot that the experimental anisotropy of the C34, C35, C37, C38 carbons is much smaller than those

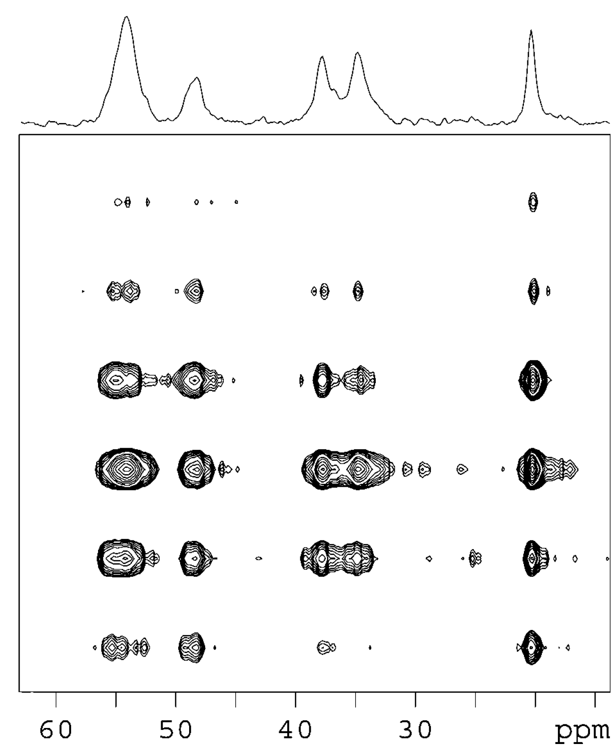

Figure 7. PASS-2D spectrum of the aliphatic region recorded with a spinning rate of 600 Hz.

TABLE 5: Values of the Calculated Chemical Shift Parameters δ_{ii} and Corresponding Anisotropic Parameters[a]

^{13}C	δ_{11} (ppm)	δ_{22} (ppm)	δ_{33} (ppm)	Ω (ppm)	κ (ppm)
C22	40	10	−3	43	−0.39
C32	48	40	12	36	0.55
C12	61	34	16	45	−0.19
C21	74	51	23	51	0.08
C11	63	59	38	25	0.66
C31	78	52	35	43	−0.23
C17	205	125	12	192	0.17
C15	202	136	9	192	0.32
C36	233	131	0	234	0.13
C37	233	130	3	230	0.10
C35	240	139	0	239	0.16
C13	219	128	9	210	0.14
C38	237	128	19	219	0.00
C34	236	153	4	232	0.29
C18	236	137	6	230	0.14
C14	236	139	20	216	0.10
C33	240	180	3	237	0.50
C16	245	164	65	180	0.09
C10	253	138	90	163	−0.42
C20	245	161	86	159	−0.05
C30	258	139	106	152	−0.57

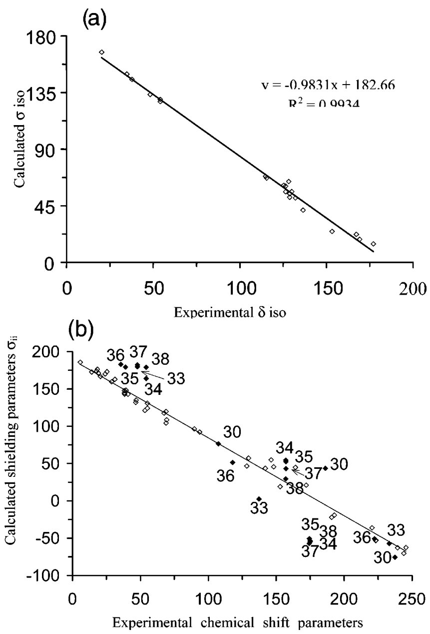

Figure 8. Correlation of (a) the experimental versus calculated isotropic values and (b) the experimental ^{13}C chemical shift δ_{ii} parameters versus the calculated ^{13}C σ_{ii} shielding parameters. In panel b, most of the scattered points are labeled.

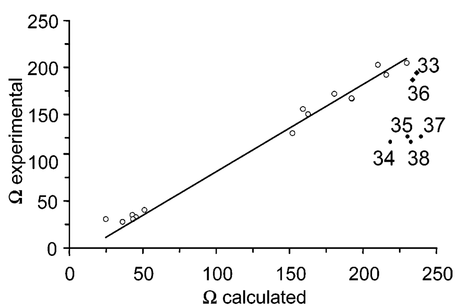

Figure 9. Correlation of the calculated Ω versus experimental Ω values. Most of the scattered points are labeled.

obtained from GIAO calculations. On the other hand, Ω for the C33 and C36 carbons roughly follow the linear correlation. To explain the origin of these discrepancies, at this stage of the studies, we assumed that molecular motion of the phenylalanine ring can reduce its anisotropy.[36] The rotational reorientation of the phenylalanine ring in the solid phase is well-established and was reported elsewhere.[37]

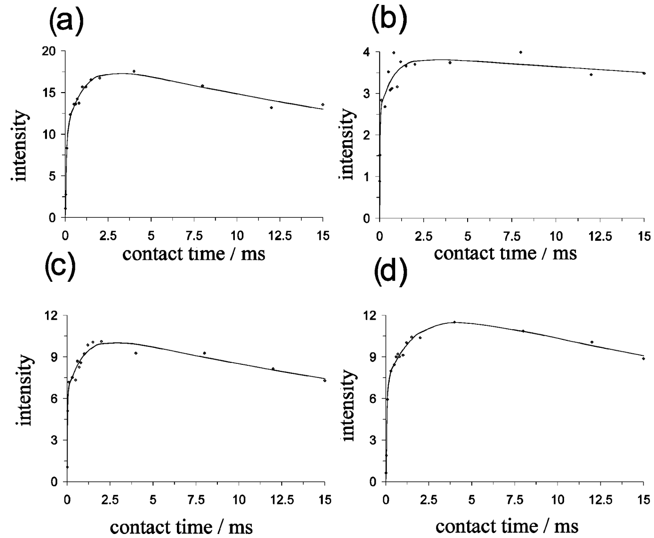

Figure 10. Cross-polarization (CP) as a function of contact time for the (a) C22, (b) C21, (c) C36, and (d) C35/C37 carbons; the data points represent the experimental data, and the solid lines correspond to the fitted curve.

3.3.3. Molecular Motions. It is well-known that analysis of the CP profile is an important source of information about the dynamics of systems under investigation. Kolodziejski and Klinowski recently reviewed this subject, showing the application of a CP kinetics approach to solve structural problems.[38] Figure 10 displays the CP curve for selected carbons of **1** as a function of contact time.

Initial analysis of the obtained data clearly revealed that the case of sample **1** is rather complex and cannot be treated by means of the classical IS model, which is expressed by eq 1:

$$M(t) = M_0\left(1 - \frac{T^{\mathrm{I}}_{\mathrm{IS}}}{T_{1\rho}}\right)^{-1}\left[\exp\left(-\frac{t}{T_{1\rho}}\right) - \exp\left(-\frac{t}{T^{\mathrm{I}}_{\mathrm{IS}}}\right)\right] \quad (1)$$

The alternative approach for interpretation of the CP kinetics is the more-advanced I−I*-S model:[37]

$$M(t) = M_0 \exp\left(-\frac{t}{T_{1\rho\mathrm{H}}}\right)\left\{1 - \lambda \exp\left(-\frac{t}{T_{\mathrm{df}}}\right) - (1-\lambda)\exp\left[-\left(\frac{3t}{2T_{\mathrm{df}}}\right) - \frac{1}{2}\left(\frac{t}{T_2}\right)^{1/2}\right]\right\} \quad (2)$$

In the I−I*-S model, two time constants characterize the increase of polarization transfer: T_2, which is dependent on the inverse direct C−H dipole−dipole interaction (which leads to a steep increase in ^{13}C polarization at starting contact times), and T_{df}, which is the spin diffusion from the neighboring protons to the direct-bonded ones (which leads to a slow increase at medium contact times). A third time constant characterizes the decrease of magnetization: $T_{1\rho\mathrm{H}}$, which is the relaxation time of the protons in the rotating frame. A fourth parameter (λ) is dependent theoretically on the number n of direct-bonded protons ($\lambda = 1/(n + 1)$); however, in practice, λ and the other CP kinetic parameters are dependent on group mobility. Therefore, λ is treated as an adjustable parameter. For CH_3 groups, a higher mobility would imply a lower CP efficiency (longer T_2 and T_{df}) and a higher proton relaxation rate ($1/T_{1\rho\mathrm{H}}$). All CP results are given in Table 6.

TABLE 6: Dynamic Parameters of 1 in the Liquid and Solid Phases[a]

^{13}C	$T_{1\rho H}$	T_{df}	T_2	λ	^{13}C T_1	^{13}C $T_1{}^a$	$\eta + 1^a$
C22	37.77	1.04	0.058	0.49	1.38	0.83	1
C32	90.50	0.04	0.119	0.63	18.48	0.49	1
C12	31.08	0.39	0.009	0.51	31.65	0.43	1
C21	37.22	0.99	0.018	0.43	43.29	0.66	1.08
C11	40.56	0.34	0.026	0.32	62.89	0.54	1
C31	38.87	0.47	0.022	0.35	62.89	0.68	1
C17	41.04	0.93	0.021	0.39	30.77	0.60	1
C15	41.04	0.93	0.021	0.39	32.57	0.60	1
C36	129.99	0.75	0.021	0.36	16.53	0.55	1.05
C35	38.49	1.79	0.053	0.48	0.60	0.73	1.15
C37	38.49	1.79	0.053	0.48	0.60	0.73	1.15
C13	31.33	0.67	0.03	0.80	35.97	1.72	1.02
C34	31.30	1.18	0.052	0.55	0.58	0.75	1.04
C38	31.30	1.18	0.052	0.55	0.58	0.75	1.04
C18	22.33	0.85	0.023	0.48	28.82	0.55	1.02
C14	40.50	0.50	0.009	0.57	31.75	0.55	1.02
C33	31.24	1.25	0.102	0.72	19.65	2.00	1.02
C16	52.31	1.05	0.105	0.61	43.67	2.63	1.15
C10	27.26	1.15	0.128	0.66	117.65	2.51	1.01
C20	25.78	1.03	0.107	0.77	80.65	2.93	1.03
C30	26.83	1.13	0.277	0.78	64.94	2.41	1

[a] Columns represent CP NMR parameters according to the I−I*-S model, spin−lattice relaxation times in the solid state (^{13}C T_1) and the liquid state ($^{13}C_1$ $T_1{}^*$), and NOE (expressed as $\eta + 1$), respectively.

Inspection of the CP data reveals that the proton spin diffusion and CP is slower for quaternary carbons (larger values of T_{df} and T_2). Consider that these parameters are also relatively large for the methyl group of D-alanine. This indicates that ^{1}H−^{1}H and ^{1}H−^{13}C dipolar interactions are weak, very likely because of the substantial mobility of this group. The C_{3v} jump of the methyl group is very common in the solid state.[39] The most intriguing information is related to data for the C34,C38 and C35,C37 carbons of phenylalanine. The values of T_{df} and T_2, which are comparable to those for the methyl group, suggest that the phenyl group of phenylalanine is under fast regime exchange.

Further evidence that confirms the unusual behavior of the phenyl ring is obtained by inspection of the data recorded with the dipolar dephasing (DD) pulse sequence.[40] This method is often used as a spectral editing technique. In the simplest approach after CP, the ^{1}H decoupler is turned off for ca. 50 μs. This is sufficient time for ^{13}C−^{1}H dipolar coupling to dephase the transverse magnetization for any ^{13}C isotope with a directly bonded ^{1}H isotope, as long as the dipolar coupling is not motionally averaged. Therefore, the lines for rigid CH and CH_2 are effectively suppressed. Figure 11a shows the DD spectrum of **1** with $\tau_D = 50$ μs. As expected, quaternary carbons and the methyl group, which is under the fast regime exchange, are observed. The CH and CH_2 carbons are suppressed, with the exception of CH aromatic signals of phenylalanine, which still give a strong response. The changes of normalized signal intensities versus the variable delay τ_D is displayed in Figure 11b. The curve, which represents CH signals of phenylalanine, is observed in the region between the quaternary carbons and the other protonated carbons. Such a picture is consistent with the data obtained from analysis of CP profiles and provides additional proof that suggests the molecular reorientation of phenylalanine.

The measurements of the spin−lattice relaxation times can be used to elucidate the dynamics of organic compounds in the solid state. The ^{13}C T_1 measurement provides information on molecular motion in the megahertz frequency range. The ^{13}C T_1 parameters measured at room temperature, by means of a Torchia sequence,[22] are collected in Table 6. Note the considerable scatter of the measured values. As predicted, the ^{13}C spin−lattice relaxation times of carboxyl/carbonyl signals are longer, compared to those of other carbons. The very short methyl group ^{13}C T_1 value was rather expected, because of fast C_{3v} reorientation of the CH_3 group, as discussed previously. The most surprising result was obtained for CH signals of phenylalanine. The ^{13}C T_1 values of the C34,C38 and C35,C37 carbons are found to be 2 times shorter, compared to the methyl group, and over 50 times shorter, compared to appropriate carbons of the tyrosine residue. This spectacular result can be observed very well in Figure 12, which displays two serial spectra recorded with a ^{13}C T_1 sequence and delays between the 90° pulses that are equal to 1 ms and 1 s, respectively.

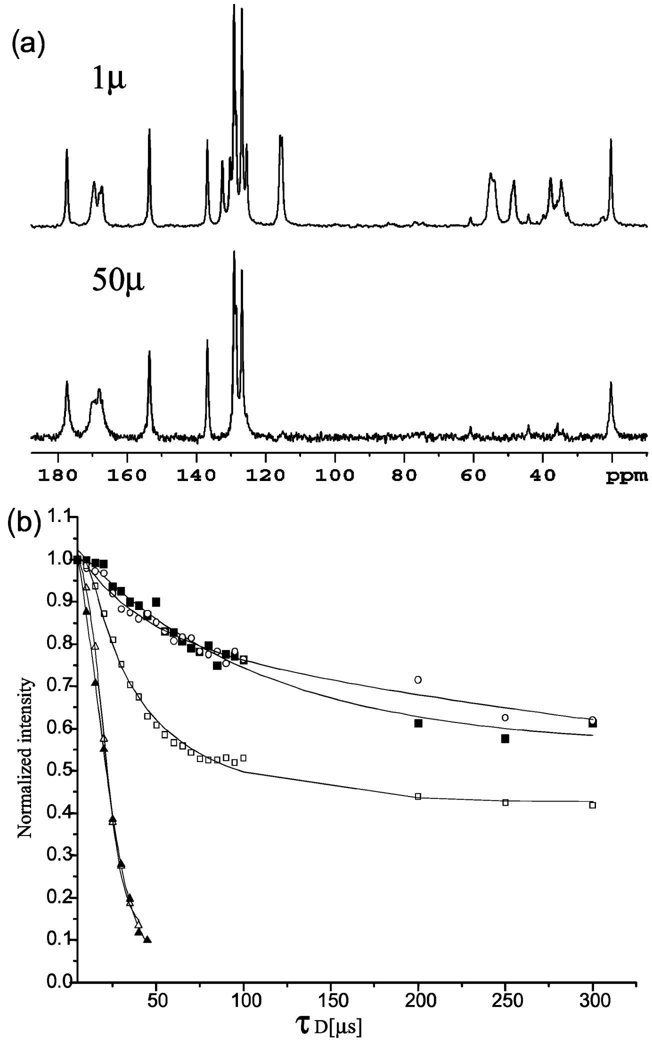

Figure 11. (a) Dipolar dephasing (DD) spectra of **1** with $\tau_D = 1$ and 50 μs. (b) Change of normalized signal intensity versus the variable delay τ_D for the (▲) C15/C17, (□) C34/C37, (△) C14, (○) C33, and (■) C16 carbons.

For the latter spectrum, the intensity of the ortho and meta CH signals of phenylalanine is suppressed to zero. This result confirmed that the phenyl group is under a fast regime exchange in the megahertz time scale. The shorter relaxation time of para CH and C quaternary carbons of phenylalanine, compared to that for the tyrosine signals, suggests additional small-amplitude motion of the peptide skeleton. This hypothesis is supported by comparing the ^{13}C T_1 values for the β-carbons of Tyr and Phe, which are found to be significantly different.

3.4. Discussion. To the best of our knowledge, in this paper, we present the first report that shows the X-ray structure of the "message domain" of dermorphin and deltorphins I, II. Our X-ray studies are correlated with NMR measurements in the

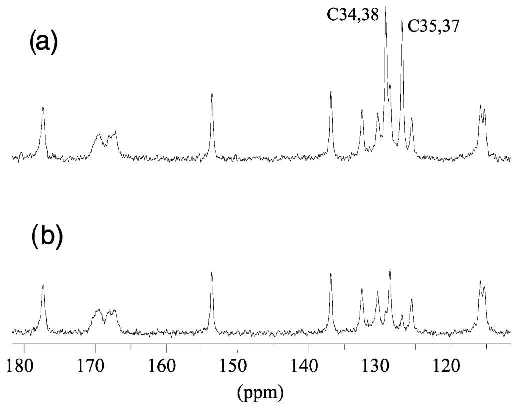

Figure 12. Serial spectra recorded with a ^{13}C T_1 sequence and a delay between 90° pulses that is equal to (a) 1 ms and (b) 1 s.

liquid and solid phases. Solid-state NMR spectroscopy is a technique that provides a link between NMR data in the solution and results obtained from the single-crystal XRD. Comparison of the isotropic chemical shifts and further structural results that characterize the geometry of the molecules in the crystal lattice offers the possibility for drawing conclusions regarding changes of conformation and configuration in both phases. Our results revealed that there is no considerable difference in the secondary structure of tripeptide **1** in both phases. Moreover, we proved that analysis of the CSTs provides detailed information about the molecular structure and dynamics of **1**.

Ramamoorthy and co-workers recently presented an exhaustive discussion on the values of the ^{13}C CST parameters of α- and β-carbons of amino acids in a series of polypeptides.[34b] In particular, much attention was given to the ^{13}C δ_{ii} values of alanine in small peptides and poly-L-alanines with different secondary structures. Although, in our case, we have the D-isomer of alanine incorporated in the structure of **1**, the ^{13}C δ_{ii} elements are very similar to those reported for the β-sheet of poly-L-alanines (the literature values are δ_{11} = 65 ppm, δ_{22} = 49 ppm, and δ_{33} = 32 ppm).[34b] The assignment of CST parameters for the Tyr and Phe residues for **1** is ambiguous, because the signals of the α-carbons are overlapped. Hence, in the PASS-2D experiment, these resonances were treated as one signal. Note that the anisotropy Ω of these signals is smaller than that of the α-carbon of D-alanine.

The CSA tensors of the C_β carbon are mainly dependent on the side chain conformation or the χ dihedral angles of residues, as well as the dynamics of the side chain. Because the methyl group in alanine rotates with a frequency of ca. 10^8 Hz around the C_{3v} axis,[41] an axially symmetric $^{13}C_\beta$ CST is predicted for alanine residues in peptides and proteins. However, as revealed by Wei et al., there are many examples where this prediction is not true.[34b] The CST values of the methyl group of D-alanine in compound **1** are not axially symmetric. The measured parameters (Table 4) are similar to those found for other small peptides (for instance, Gly-Ala). Note the distinction of the CST parameters for β-carbons of C12 and C32. These differences can be related with the distinction of the χ torsional angles, which are equal to 173.22° and 57.84°, respectively. Interestingly, the theoretical calculations of the shielding parameters suggest an even larger distinction of the ^{13}C δ_{ii} parameters. These differences can be understood if we assume small-amplitude motions of the aliphatic groups in the solid phase, which are not considered in the calculations.

Analysis of the values of the ^{13}C δ_{ii} parameters and correlation with the calculated data obtained by means of the DFT GIAO method can provide important information about local molecular motion. The observed discrepancy between the experimental and theoretical values for phenylalanine aromatic-ring carbons is explained in terms of fast molecular reorientation of the phenyl group. The collapse of the CST from its rigid lattice values, which is related to the molecular motion, is known and was reported elsewhere.[42] The principal elements of the ^{13}C σ_{ii} of the C30 carboxyl site require a short comment. Figure 8b shows that the σ_{11} and σ_{22} components significantly deviate from the fitted line. Similar results were reported for the zwitterionic amino acids L-theronine and L-tyrosine. As shown by de Dios et al., when zwitterions are included in the calculation, which are represented as point charges, significant improvements in the carboxyl ^{13}C tensor components are obtained.[43]

The molecular dynamics of opioid peptides in the solid phase is still one of the challenging problems. Naito and co-workers investigated backbone motion and side-chain dynamics for different polymorphs of enkephalins, using high-resolution solid-state NMR spectroscopy and line-shape analysis of the ^{2}H nucleus for selectively labeled samples.[44] As concluded, relaxation parameters are tools that provide detailed information about the frequency and amplitude of molecular motion. In case of **1**, the CP kinetics and ^{13}C spin−lattice relaxation times show that the phenyl group of the phenylalanine residue is under fast regime exchange. The significantly shorter ^{13}C T_1 values of the C34,C38 and C35,C37 carbons, compared to that of the C36 carbon, suggest rapid flip-flop or diffusional motion of the phenyl ring around 1−4 axes. Similar behavior of the phenyl ring was reported for enkephalins.[44] However, the fact that the dynamics of aromatic rings of tyrosine and phenylalanine is dramatically different seems to be a unique feature of the compound under investigation. Moreover, the small-amplitude motion of the tripeptide backbone—in particular, in the C part of **1**—cannot be excluded. The presence of motions could be also characterized by proton spin−lattice relaxation times in the rotating frame $T_{1\rho}^{\mathrm{H}}$. The very long $T_{1\rho}^{\mathrm{H}}$ that is observed for **1** means that the spin-diffusion process is not effective in this case, probably because of the presence of rapid motions, as detected by ^{13}C T_1 (vide supra).

Finally, we were prompted to answer the question whether distinction of the molecular motion of the backbone and side chain groups can be also observed in the liquid phase. Chenon and Werbelow recently reported the solution dynamics of deltorphin I, using NMR relaxation measurements.[45] In particular, the two residues D-alanine and glycine, each of which have very different mobility, were examined. ^{13}C T_1 relaxation times of **1** in a methanol:water solution (1/1 v/v), measured by means of a SUFIR [21] sequence, are collected in Table 6. As predicted, the ^{13}C T_1 of quaternary atoms are considerably longer, compared to other carbons. The most interesting information comes from the analysis of the ^{13}C T_1 of CH aromatic carbons. For the C14,C18, C15,C17, and C36 carbons, the relaxation times are similar, whereas for the C34,C38 and C35,C78 carbons, the relaxation times are slightly longer. These results suggest local motion of the phenyl ring around the C33,C36 axis also in the liquid phase. Note the relatively long ^{13}C T_1 of the methyl group of D-alanine, which undergoes a C_{3v} jump. The case of **1** is beyond the scope of the "extreme narrowing case"; therefore, quantitative interpretation of the relaxation parameters, in terms of the overall and local motion of the side groups, requires a more-advanced mathematical approach and is treated as a separate project.

4. Conclusions

In this paper, we have demonstrated the complementarity and the power of the multiple technique approach in the structural studies of peptides. X-ray crystallography, combined with NMR spectroscopy in the liquid and solid states and DFT GIAO calculations, provides detailed information on the structure and dynamics of the "message" sequence of the entitled opioid peptides. Our studies on the overall and local motions of side groups in both phases create new questions regarding the role of the stereochemisty of alanine in a tripeptide unit. Stereochemistry seems to be a crucial factor in determining the local molecular motion of **1**. The methyl group of D-alanine that is due to C−H$\cdots\pi$ interaction only with the phenyl group of tyrosine, strengthened by steric hindrance, can be considered to make the N-terminal part of the peptide rigid. Very likely, these effects are absent in the case of L-alanine. Recall that analogous peptides that have L-alanine in their structure do not reveal biological activity. The open question remains in regard to whether observation regarding the distinction of the phenyl group dynamics for **1** can be extended onto opioid peptides, e.g., dermorphin and deltorphins I, II.

Acknowledgment. The authors are grateful to the Polish Committee for Scientific Research, KBN (under Grant No. 3 T09A02619) for financial support. M.J.P. is thankful to Professors S. Jankowski and J. Zabrocki from Technical University of Łódź for encouraging study of the problem of opioid peptides. The X-ray data was collected on the X-13 beam line at the European Molecular Biology Laboratory (EMBL) in Hamburg, Germany.

References and Notes

(1) (a) Okada, Y.; Tsuda, Y.; Bryant, S. D.; Lazarus, L. H. *Vitam. Horm. (San Diego)* **2002**, *65*, 257. (b) Pogozheva, I. D.; Lomize, A. L.; Mosberg, H. I. *Biophys. J.* **1998**, *75*, 612. (c) Smith, A. P.; Lee, N. M. *Life Sci.* **2003**, *73*, 1873.

(2) Snyder, S. H.; Pasternak, G. W. *Trends Pharmacol. Sci*. **2003**, *24*, 198.

(3) Deschamps, J. R.; George, C.; Flippen-Anderson, J. L. *Biopolymers* **1996**, *40*, 121.

(4) Hruby, V. J.; Agnes, R. S. *Biopolymers* **1999**, *51*, 391.

(5) Daly, J. W.; Caceres, J.; Moni, R. W.; Gusovky, F.; Moos, M.; Seamon, K. B.; Milton, K.; Myers, C. W. *Pharmacology* **1992**, *89*, 10960.

(6) Montecucchi, P. C.; de Castiglione, R.; Piani, S.; Gozzini, L.; Erspamer, V. *Int. J. Pept. Protein Res.* **1981**, *17*, 275.

(7) Erspamer, V. *Int. J. Dev. Neurosci*. **1992**, *10*, 3.

(8) Hong, J.; Rhoheng, Z.; Xiaoyu, H.; Luhua, L.; Xiaojie, X. *Biochem. Biophys. Res. Commun.* **1995**, *207*, 99.

(9) Mignogna, G.; Severini, C.; Simmaco, M.; Negri, L.; Erspamer, G. F.; Kreil, G.; Barra, D. *FEBS Lett*. **1992**, *302*, 151.

(10) Temussi, P. A.; Picone, D.; Tancred, T.; Tomatis, R.; Salvadori, S.; Marastoni, M.; Balboni, G. *FEBS Lett*. **1989**, *247*, 283.

(11) Tancredi, T.; Temussi, P. A.; Picone, D.; Amodeo, P.; Tomatis, R.; Salvadori, S.; Marastioni, M.; Santaga, V.; Balboni, G. *Biopolymers* **1991**, *31*, 751.

(12) Tourwe, D.; Verschueren, K.; Frycia, A.; Davis, P.; Porreca, F.; Hruby, V. J.; Toth, G.; Jaspers, H.; Verheyden, P.; Van Binst, G. *Biopolymers* **1996**, *38*, 1.

(13) (a) Castiglione-Morelli, M. A.; Lelj, F.; Pastore, A.; Salvadori, S.; Tancredi, T.; Tomatis, R.; Trivellone, E.; Temussi, P. A. *J. Med. Chem.* **1987**, *30*, 2067. (b) Nikiforovich, G. V.; Hruby, V. J.; Prakash, O.; Gehrig, A. *Biopolymers* **1991**, *31*, 941. (c) Segawa, M.; Ohno, Y.; Doi, M.; Ishida, T.; Iwashita, T. *Int. J. Peptide Res*. **1995**, *46*, 37.

(14) Sheldrick, G. M.; Kruger, G. M.; Goddard, R. SHELXS-86. Structure Solution Program. *Acta Crystallogr., Sect. A: Found. Crystallogr.* **1990**, *A46*, 467−473.

(15) Sheldrick, G. M. *SHELXL-93, Program for Crystal Structure Refinement*; University of Göttingen: Göttingen, Germany, 1993.

(16) Morcombe, C. R.; Zilm, K. W. *J. Magn. Reson*. **2003**, *162,* 479.

(17) *Win-NMR, Version 6.0*; Bruker-Franzen Analytik GmbH: Bremen, Germany, 1993.

(18) Antzutkin, O. N.; Shekar, S. C.; Levitt, M. H. *J. Magn. Reson.* **1995**, *115*, 7.

(19) Bak, M.; Rasmussen, J. T.; Nielsen, N. C. *J. Magn. Reson*. **2000,** *147*, 296.

(20) Frisch, M. J.; Trucks, G. W.; Schlegel, H. B.; Scuseria, G. E.; Robb, M. A.; Cheeseman, J. R.; Zakrzewski, V. G.; Montgomery, J. A., Jr.; Stratmann, R. E.; Burant, J. C.; Dapprich, S.; Millam, J. M.; Daniels, A. D.; Kudin, K. N.; Strain, M. C.; Farkas, O.; Tomasi, J.; Barone, V.; Cossi, M.; Cammi, R.; Mennucci, B.; Pomelli, C.; Adamo, C.; Clifford, S.; Ochterski, J.; Petersson, G. A.; Ayala, P. Y.; Cui, Q.; Morokuma, K.; Malick, D. K.; Rabuck, A. D.; Raghavachari, K.; Foresman, J. B.; Cioslowski, J.; Ortiz, J. V.; Stefanov, B. B.; Liu, G.; Liashenko, A.; Piskorz, P.; Komaromi, I.; Gomperts, R.; Martin, R. L.; Fox, D. J.; Keith, T.; Al-Laham, M. A.; Peng, C. Y.; Nanayakkara, A.; Gonzalez, C.; Challacombe, M.; Gill, P. M. W.; Johnson, B. G.; Chen, W.; Wong, M. W.; Andres, J. L.; Head-Gordon, M.; Replogle, E. S.; Pople, J. A. *Gaussian 98*, revision A.6; Gaussian, Inc.: Pittsburgh, PA, 1998.

(21) Canet, D.; Brondeau, J.; Elbayed, K. *J. Magn. Reson*. **1988**, *77*, 483.

(22) Torchia, D. A. *J. Magn. Reson*. **1978**, *30*, 613.

(23) Tooyama, I.; Abe, H.; Renda, T. G. *Peptides* **2000**, *21*, 1649.

(24) Brandl, M.; Weiss, M. S.; Jabs, A.; Suhnel, J.; Hilgenfeld, R. *J. Mol. Biol*. **2001**, 16, *307*, 357.

(25) Metz, G.; Wu, X.; Smith, S. O. *J. Magn. Reson., Ser. A* **1994**, *110*, 219.

(26) Bennett, A. W.; Rienstra, C. M.; Auger, M.; Lakshmi, K. V.; Griffin, R. G. *J. Chem. Phys.* **1995**, *16*, 103.

(27) (a) Hu, J.; Wang, W.; Liu, F.; Solum, M. S.; Alderman, D. W.; Pugmire, R. J. *J. Magn. Reson., Ser. A* **1995**, *113*, 210. (b) Alderman, D. W.; McGeorge, G.; Hu, J. Z.; Pugmire, R. J.; Grant, D. M. *Mol. Phys*. **1998**, *95*, 1113. (c) Frydman, L.; Chingas, G. C.; Lee, Y. K.; Grandinetti, P. J.; Eastman, M. A.; Barral, G. A.; Pines, A. *J. Chem. Phys*. **1992**, *97*, 480. (d) Kolbert, A. C.; Griffin, R. G. *Chem. Phys. Lett*. **1990**, *166*, 87.

(28) Antzutkin, O. N. *Prog. NMR Spectrosc*. **1999**, *35*, 203.

(29) Dixon, W. T. *J. Chem. Phys.* **1982**, *77*, 1800.

(30) Ye, C.; Fu, R.; Hu, J.; Hou, L.; Ding, S. *Magn. Reson. Chem*. **1993**, *31*, 699.

(31) Gu, Z. T.; McDermott, A. *J. Am. Chem. Soc.* **1993**, *115*, 4282.

(32) Gu, Z. T.; Zambrano, R.; McDermott, A. *J. Am. Chem. Soc*. **1994**, *116*, 6368.

(33) Ando, I.; Kuroki, S.; Kurosu, H.; Yamanobe, T. *Prog. Nucl. Magn. Reson. Spectrosc.* **2001**, *39*, 79 and references therein.

(34) (a) Oldfield, E. *Annu. Rev. Phys. Chem.* **2002**, *53*, 349 and references therein. (b) Wei, Y.; Lee, D. K.; Ramamoorthy, A. *J. Am. Chem. Soc.* **2001**, *123,* 6118.

(35) (a) Grant, D. M.; Facelli, J. C.; Alderman, D. W.; Sherwood, M. H. In *Nuclear Magnetic Shielding and Molecular Structure*; Tossell, J. A., Ed.; Kluwer Academic Publishers: Dordrecht, The Netherlands, 1993; p 367. (b) Malkin, V. G.; Malkina, O. L.; Eriksson, L. A.; Salahub, D. R. Modern Density Functional Theory: A Tool for Chemistry. In *Theoretical and Computational Chemistry*, Vol. 2; Seminaro, J. M., Politzer, P., Eds.; Elsevier, Amsterdam, 1995.

(36) Inglefield, P. T.; Amicim, R. M.; O'Gara, J. F.; Hung, C.-C.; Jones, A. A. *Macromolecules* **1983**, *16*, 1552.

(37) (a) Gall, C. M.; Diverdi, J. A.; Opella, S. J. *J. Am. Chem. Soc.* **1981**, *103*, 5039. (b) Kinsey, R. A.; Kintanar, A.; Tsai, M. D.; Smith, R. L.; Janes, N.; Oldfield, E. *J. Biol. Chem.* **1981**, *256*, 4146. (c) Hiyama, Y.; Silverton, J. V.; Torchia, D. A.; Gerig, J. T.; Hammond, S. J. *J. Am. Chem. Soc.* **1986**, *108*, 2715.

(38) Kolodziejski, W.; Klinowski, J. *Chem. Rev.* **2002**, *102*, 613.

(39) Straus, S. K.; Bremi, T.; Evnat, R. R. *J. Biomol. NMR* **1997**, *10*, 119.

(40) (a) Alla, M.; Lippmaa, E. *Chem. Phys. Lett*. **1976**, *37*, 260. (b) Opella, S. J.; Frey, M. H. *J. Am. Chem. Soc*. **1979**, *37*, 260. (c) Zilm, K. W. In *Spectral Editing Techniques: Hydrocarbon Solids*; Grant, D. M., Harris, R. K., Eds.; Encyclopedia of Nuclear Magnetic Resonance, Vol. VII; Wiley: Chichester, U.K., 1996; 4498 pp.

(41) Beshah, K.; Olejniczak, E. T.; Griffin, R. G. *J. Chem. Phys.* **1987**, *86*, 4730.

(42) Lyerla, J. R. High-Resolution NMR of Glassy Amorphous Polymers (Chapter 3). In *High-Resolution NMR Spectroscopy of Synthetic Polymers in Bulk*; Komorowski, R. A., Ed.; VCH Publishers: Deerfield Beach, FL, 1986; pp 63−119.

(43) de Dios, A. C.; Laws, D. D.; Oldfield, E. *J. Am. Chem. Soc*. **1994**, *116*, 7784.

(44) (a) Kamihira, M.; Naito, A.; Tuzi, S.; Saito, H. *J. Phys. Chem. A* **1999**, *103*, 3356. (b) Kamihira, M.; Naito, A.; Nishimura, K.; Tuzi, S.; Saito, H. *J. Phys. Chem. B* **1998**, *102*, 2826.

(45) Werbelow, L. G.; Chenon, T. M. *J. Am. Chem. Soc.* **2002**, *124*, 14066.

(46) Data from the Cambridge Crystallographic Data Centre is available free of charge via the Internet, at www.ccdc.cam.ac.uk/-const/retrieving.html, as well as via E-mail (deposit@ccdc.cam.ac.uk), postal service (Cambridge Crystallographic Data Centre, 12, Union Road, Cambridge CB2 1EZ, U.K.), or fax (+44-1223/336-033).